Low mass dilepton production at ultrarelativistic energies

E.L. Bratkovskaya [a,*], W. Cassing [b], O. Linnyk [a]

[a] *Frankfurt Institute for Advanced Studies, Johann Wolfgang Goethe University, Ruth-Moufang-Str. 1, 60438 Frankfurt am Main, Germany*
[b] *Institut für Theoretische Physik, Universität Giessen, Heinrich-Buff-Ring 16, D-35392 Giessen, Germany*

A B S T R A C T

Dilepton production in pp and Au + Au nucleus–nucleus collisions at $\sqrt{s} = 200$ GeV as well as in In + In and Pb + Au at 158 A GeV is studied within the microscopic HSD transport approach. A comparison to the data from the PHENIX Collaboration at RHIC shows that standard in-medium effects of the ρ, ω vector mesons—compatible with the NA60 data for In + In at 158 A GeV and the CERES data for Pb + Au at 158 A GeV—do not explain the large enhancement observed in the invariant mass regime from 0.2 to 0.5 GeV in Au + Au collisions at $\sqrt{s} = 200$ GeV relative to pp collisions.

© 2008 Elsevier B.V.

While the properties of hadrons are rather well known in free space (embedded in a nonperturbative QCD vacuum) the masses and lifetimes of hadrons in a baryonic and/or mesonic environment are subject of current research in order to achieve a better understanding of the strong interaction and the nature of confinement. In this context the modification of hadron properties in nuclear matter are of fundamental interest (cf. Refs. [1–5]) since QCD sum rules [2,3,6] as well as QCD inspired effective Lagrangian models [1,4,7–10] predict significant changes, e.g. of the vector mesons (ρ, ω and ϕ) with the nuclear density ρ_N and/or temperature T [11, 12].

A modification of vector mesons has been seen experimentally in the enhanced production of lepton pairs above known sources in nucleus–nucleus collisions at Super-Proton-Synchroton (SPS) energies [13,14]. As proposed by Li, Ko, and Brown [15] and Ko et al. [16] the observed enhancement in the invariant mass range $0.3 \leqslant M \leqslant 0.7$ GeV might be due to a shift of the ρ-meson mass following Brown/Rho scaling [1] or the Hatsuda and Lee sum rule prediction [2]. The microscopic transport studies in Refs. [11,17–19] for these systems have given support for this interpretation. On the other hand also more conventional approaches that describe a

melting of the ρ-meson in the medium due to the strong hadronic coupling (along the lines of Refs. [9,10]) have been found to be compatible with the early CERES data [12,17,20]. This ambiguous situation has been clarified to some extent in 2006 by the NA60 Collaboration since the invariant mass spectra for $\mu^+\mu^-$ pairs from In + In collisions at 158 A GeV favored the 'melting ρ' scenario [21]. Also the more recent data from the CERES Collaboration (with enhanced mass resolution) [22] show a preference for the 'melting ρ' picture.

In 2007 the PHENIX Collaboration has presented first dilepton data from pp and Au + Au collisions at Relativistic-Heavy-Ion-Collider (RHIC) energies of $\sqrt{s} = 200$ GeV [23] which show an even larger enhancement in Au + Au reactions (relative to pp collisions) in the invariant mass regime from 0.15 to 0.6 GeV than the data at SPS energies [21,22]. The question arises if this sizeable enhancement might also be attributed to in-medium modifications of the ρ and ω mesons as at SPS energies [11,12] or if new radiative channels from the strong Quark–Gluon Plasma (sQGP) have been seen.

The answer to this question is nontrivial due to the nonequilibrium nature of the heavy-ion reactions and covariant transport models have to be incorporated to disentangle the various sources that contribute to the final dilepton spectra seen experimentally. In this study we aim at contributing to this task employing an up-to-date relativistic transport model (HSD) that incorporates the relevant off-shell dynamics of the vector mesons. The HSD transport

* Corresponding author.
E-mail address: elena.bratkovskaya@th.physik.uni-frankfurt.de
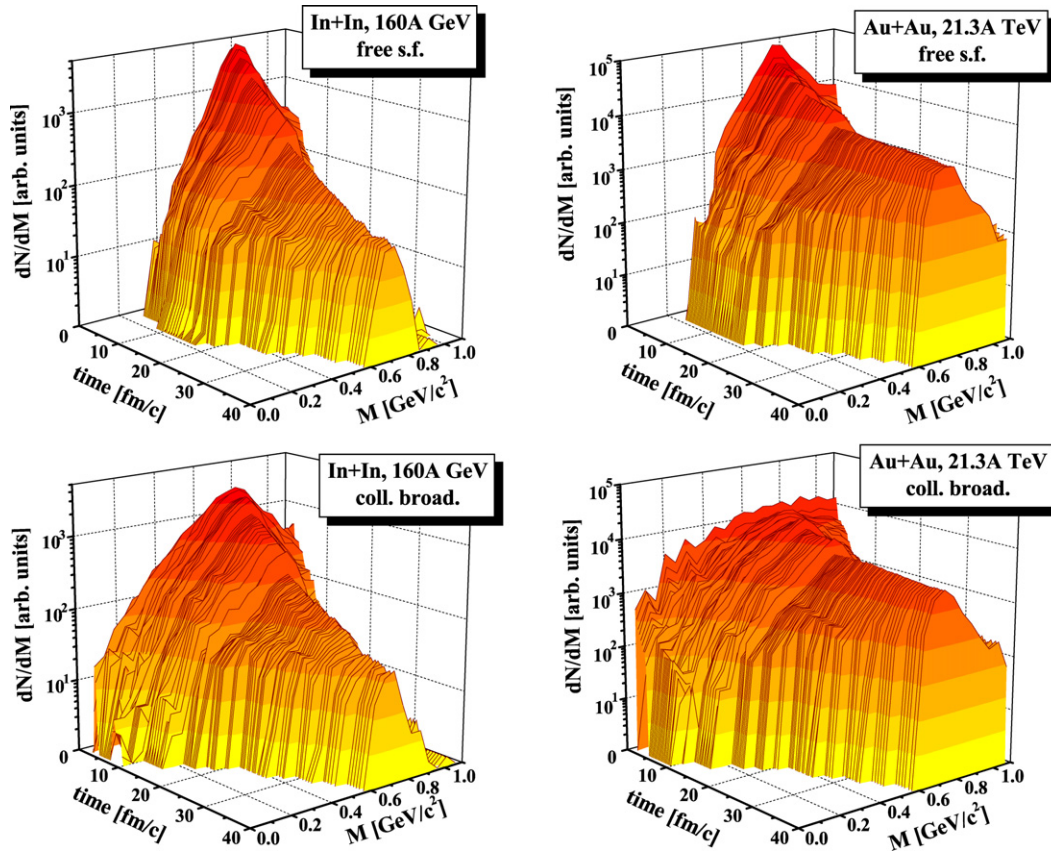(E.L. Bratkovskaya).

Fig. 1. Time evolution of the mass distribution of ρ mesons for central ($b = 0.5$ fm) In + In collisions at 160 A GeV (left part) and for Au + Au collisions at 21.3 A TeV (right part) for the free spectral function (upper plots) and for the 'collisional broadening' scenario (lower plots).

model [11,18,24] has been used for the description of pA and AA collisions from SIS to RHIC energies and lead to a fair reproduction of hadron abundancies, rapidity distributions and transverse momentum spectra. We recall that in the HSD approach nucleons, Δ's, $N^*(1440)$, $N^*(1535)$, Λ, Σ and Σ^* hyperons, Ξ's, Ξ^*'s and Ω's as well as their antiparticles are included on the baryonic side whereas the 0^- and 1^- octet states are incorporated in the mesonic sector. Inelastic baryon–baryon (and meson–baryon) collisions with energies above $\sqrt{s}_{th} \simeq 2.6$ GeV (and $\sqrt{s}_{th} \simeq 2.3$ GeV) are described by the FRITIOF string model [25] whereas low energy hadron–hadron collisions are modeled in line with experimental cross sections. Low energy cross sections such as threshold meson production in proton–neutron (pn) collisions—which are scarcely available from experiments—are fixed by proton–proton (pp) cross sections and isospin factors emerging from pion-exchange diagrams. Since we address ultrarelativistic collisions at SPS and RHIC energies such 'low energy uncertainties' are of minor relevance here. As pre-hadronic degrees of freedom HSD includes 'effective' quarks (antiquarks) and diquarks (antidiquarks) which interact with cross sections in accordance with the constituent quark model (cf. Refs. [26]).

Compared to our earlier studies in Refs. [11,20] a couple of extensions have been implemented such as

- off-shell dynamics for vector mesons—according to Refs. [27]—and an extended set of vector meson spectral functions [28],
- extension of the LUND string model to include 'modified' spectral functions for the hadron resonances in the string decays.

As demonstrated in Ref. [28] the off-shell dynamics is particularly important for resonances with a rather long lifetime in vacuum but strongly decreasing lifetime in the nuclear medium (especially

ω and ϕ mesons) but also proves vital for the correct description of dilepton decays of ρ mesons with masses close to the two pion decay threshold.[1] For a detailed description of the various hadronic channels included for dilepton production as well as the off-shell dynamics we refer the reader to Ref. [28] where we have focused on e^+e^- production in the 1 to 2 A GeV energy range.

Before we step to a comparison with experimental data we show in Fig. 1 the time evolution of the mass distribution of ρ mesons for central ($b = 0.5$ fm) In + In collisions at 160 A GeV (left part) and for Au + Au collisions at 21.3 A TeV (right part) for the free ρ spectral function (upper plots) and the 'collisional broadening' scenario (lower plots). In the free case there are no mass components below $2m_\pi$ whereas in the 'collisional broadening' scenario the ρ mass distribution extends down to twice the electron mass. The ρ mass distributions for times $t > 15$ fm/c essentially show the width due to the $\rho \to \pi\pi$ decay in vacuum which is delayed at the RHIC energy due to significantly larger Lorentz γ factors (with respect to the calculational frame). In the collisional broadening case (lower plots) we observe a substantially larger width in the initial ρ meson mass distribution at the RHIC energy due to a larger baryon + antibaryon density for the heavier Au + Au system and a higher ρ + meson scattering rate. The corresponding results on dilepton spectra—within the experimental acceptance and mass resolution—will be shown below.

We mention that also finite temperature effects lead to a sizable broadening of the vector mesons spectral functions (also at baryon chemical potential $\mu_B = 0$). This is essentially due to vector meson scattering with mesons which may contribute to the total

---

[1] This will be of particular importance in comparison to the low mass dileptons from PHENIX.
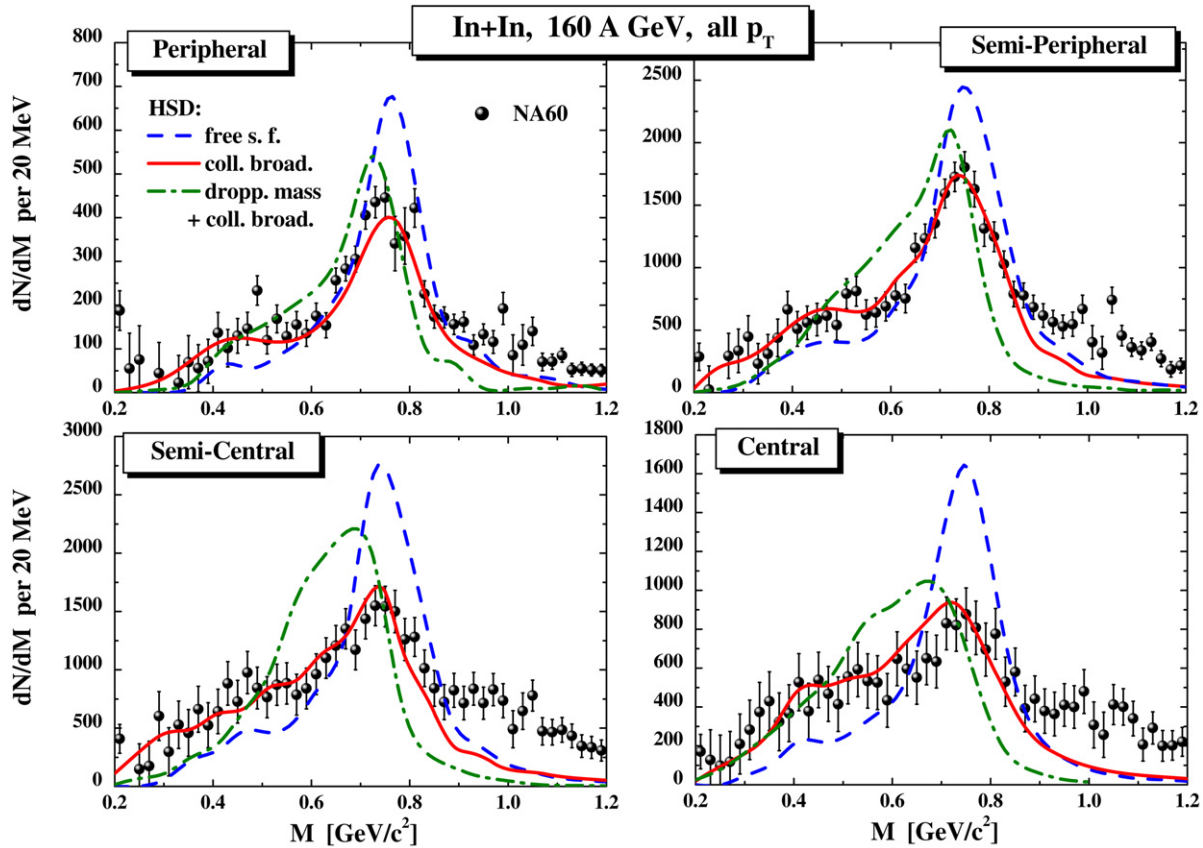
Fig. 2. The HSD results for the mass differential dilepton spectra from the direct ρ meson decay in case of In + In at 158 A GeV for peripheral, semi-peripheral, semi-central and central collisions in comparison to the excess mass spectrum from NA60 [21]. The actual NA60 acceptance filter and mass resolution have been incorporated [31]. The solid lines show the HSD results for a scenario including the collisional broadening of the ρ-meson whereas the dashed lines correspond to calculations with 'free' ρ spectral functions for reference. The dash-dotted lines represent the HSD calculations for the 'dropping mass + collisional broadening' model (see text).

width by 70–80 MeV at a temperature of ∼170 MeV according to the early work by Haglin [29]. For the present study we use a simplified modeling of the collisional broadening by meson scattering which discards an explicit consideration of such 'temperature effects' in the parametrization of the vector-meson spectral functions (cf. Ref. [28]). However, the 'temperature effects' are partly accounted here by explicit meson–meson interactions which lead to a dynamical broadening in the vector meson mass distribution.

Let us directly go over to the actual results from HSD for In + In collisions at 160 A GeV which are displayed in Fig. 2 for peripheral, semi-peripheral, semi-central and central collisions following the centrality definition of the NA60 Collaboration [21,30,31]: all measured events have been separated into 4 centrality bins according to their charged particle multiplicity $dN_{ch}/d\eta$ measured in the pseudorapidity interval $3 \leqslant \eta \leqslant 4.2$ (cf. Ref. [30] for details): bin 1 (central) – $170 \leqslant dN_{ch}/d\eta \leqslant 240$; bin 2 (semi-central) – $110 \leqslant dN_{ch}/d\eta \leqslant 170$; bin 3 (semi-peripheral) – $30 \leqslant dN_{ch}/d\eta \leqslant 110$; bin 4 (peripheral) – $4 \leqslant dN_{ch}/d\eta \leqslant 30$. By computing $dN_{ch}/d\eta$ within HSD for the same pseudorapidity interval we obtain a direct correspondence of the centrality bins with the impact parameter intervals: bin 1 (central) – $b \leqslant 3.5$ fm; bin 2 (semi-central) – $3.5 \leqslant b \leqslant 5.5$ fm; bin 3 (semi-peripheral) – $5.5 \leqslant b \leqslant 8.5$ fm; bin 4 (peripheral) – $b \geqslant 8.5$ fm which we used as centrality criteria for our calculations. We note, furthermore, that the experimental data in Fig. 2 correspond to the 'excess mass spectra', which are extracted from the measured dilepton yields by subtracting the 'cocktail' contribution from the η, ω, ϕ decays [21]. Such a procedure allows to 'separate' the contribution of the ρ mesons which is dominant in the mass region $0.25 \leqslant M \leqslant 0.9$ GeV/c^2 over other dilepton sources. Following Ref. [21] we compare in Fig. 2 the cor-

responding NA60 data for the excess mass spectra with the HSD calculations for the dilepton yield from the direct ρ mesons, where the normalization to the data is performed with respect to the integral yield from 0.2 to 0.9 GeV for all scenarios considered. Note that an absolute normalization to the NA60 data—contrary to the systems discussed below—is not yet available and we thus focus on a 'shape' analysis.

The dashed lines give the dilepton mass spectra for the direct ρ meson decays when incorporating only the vacuum ρ-spectral function in all hadronic reaction processes. These reference spectra overestimate the data in the region of the ρ-meson pole mass and underestimate the experimental spectra in the region below (and above) the pole mass such that in-medium modifications can clearly be identified. The solid lines show the result from HSD in the 'collisional broadening' scenario where no shift of the ρ pole mass is incorporated but an increase of the ρ-meson width due to hadronic collisions proportional to the baryon density ρ_B (calculated as $\rho_B^2(x) = j^\mu(x)j_\mu(x)$ with $j^\mu(x)$ denoting the baryon 4-current). The dash-dotted lines represent the HSD calculations for the 'dropping mass + collisional broadening' model where the ρ mass has been dropped with baryon density in accordance with Eq. (10) in Ref. [28]. An explicit representation of the ρ- and ω-meson spectral functions employed here is presented in Fig. 2 of Ref. [28]. As can be seen from Fig. 2 the dilepton mass spectrum is rather well described up to invariant masses of 0.9 GeV in the 'collisional broadening' scenario. For higher invariant masses the data signal additional contributions. This result is practically identical to the calculations of van Hees and Rapp [32] in the expanding fireball model—when incorporating the spectral function from Ref. [9]—and demonstrates that the dominant in-medium ef-
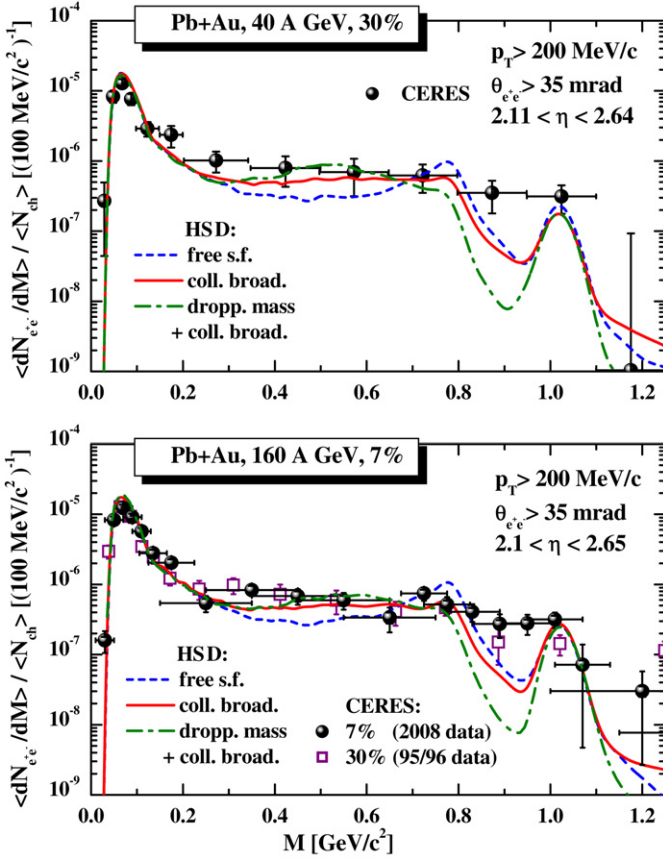
Fig. 3. The HSD results for the mass differential dilepton spectra in 30% central Pb + Au collisions at 40 *A* GeV (upper part) and 7% central collisions at 158 *A* GeV (lower part) in comparison to the data from CERES [22]. The dashed lines show the results for vacuum spectral functions (for ρ, ω, ϕ) whereas the solid lines correspond to the 'collisional broadening' scenario. The dash-dotted lines represent the HSD calculations for the 'dropping mass + collisional broadening' model (see text).

fect seen in the $\mu^+\mu^-$ spectra from NA60 is a broadening of the ρ meson. The 'dropping mass + collisional broadening' model performs worse since it shifts too much strength to lower invariant dilepton masses. Note, however, that a reduced dropping of the vector-meson masses might be also compatible with the present data sets.

In Ref. [33] a very detailed analysis of the NA60 data has been performed and shown that the additional yield above 0.9 GeV partly is due to open charm decays, four-pion collisions or 'quark–antiquark' annihilation. We mention that our HSD calculations give only a small contribution from $\pi + a_1$ collisions in this invariant mass range but a preliminary study within the Parton–Hadron-String-Dynamics (PHSD) model [34] suggests that—apart from open charm decays—the extra yield seen experimentally by NA60 should be due to massive 'quark–antiquark' annihilations. Since this question is presently open and discussed controversially [35–39] we concentrate on low mass dilepton pairs in the following.

The next step in our study is related to an update of the HSD calculations in comparison to the recent data from the CERES Collaboration [22] (with enhanced mass resolution). In Fig. 3 we present the HSD results for the mass differential dilepton spectra in 30% central Pb + Au collisions at 40 *A* GeV (upper part) and 7% central collisions at 158 *A* GeV (lower part) in comparison to the data from CERES [22]. The experimental dilepton yields in Fig. 3 are normalized to the average number of charged particles for the corresponding centrality in the CERES acceptance: for 7% most central 158 *A* GeV events $\langle N_{ch} \rangle = 177$ and for 30%

central 40 *A* GeV events $\langle N_{ch} \rangle = 216$ in the pseudo-rapidity interval $2.1 \leqslant \eta \leqslant 2.65$. Correspondingly, the calculated dilepton yields have been also normalized to $\langle N_{ch} \rangle$ obtained directly from the HSD calculations which are in good agreement with the measured numbers indicated above. The dashed lines in Fig. 3 show the results in case of vacuum spectral functions (for ρ, ω, ϕ) whereas the solid lines correspond to the 'collisional broadening' scenario. As in Fig. 2 the dash-dotted lines represent the HSD calculations for the 'dropping mass + collisional broadening' model. Similar to the In + In case the experimental data agree with the calculations employing the 'collisional broadening' scenario (also in line with Ref. [33]). However, the CERES data also compare reasonably well with the 'dropping mass + collisional broadening' model up to invariant masses of 0.8 GeV.

On the other hand, the HSD model underpredicts the yield between the ω and ϕ peaks which might again be attributed to possible contributions from 'quark–antiquark' annihilations etc. We mention that in Ref. [18] we showed that this invariant mass region is very sensitive to the in-medium scenario since the simple 'dropping mass' picture provided a strong shift of the dilepton yield to the low mass regime and a strong reduction of the dilepton yield at $M \sim 0.9$ GeV whereas the 'collisional broadening' scenario gave a much larger contribution at $M \sim 0.9$ GeV. The 'dropping mass + collisional broadening' model (dot-dashed lines) shows a similar but less pronounced trend. Thus detailed measurements of this mass regime with high resolution will provide interesting constraints on the in-medium scenarios and might as well indicate possible contributions from partonic degrees of freedom— e.g. quark–antiquark annihilation or gluon-Compton scattering— already at SPS energies. A more detailed investigation within the PHSD approach will be presented in the near future.

In addition to the total yield shown in Fig. 3 the CERES Collaboration presented also the 'excess' yield (similar to NA60) defined by the dilepton yield after subtraction of the hadronic cocktail [22]. The hadronic 'cocktail' is composed by the sum of π^0, η, ω, η' Dalitz decays and direct decays of ω and ϕ mesons to dileptons. Thus, the residual dilepton yield might be attributed to the ρ meson contribution. The experimental excess yield is shown in Fig. 4 (solid dots with errorbars) in comparison to the HSD calculations: the dashed line shows the result for the vacuum ρ spectral function, the solid line corresponds to the 'collisional broadening' scenario and the dash-dotted line represents the HSD calculations for the 'dropping mass + collisional broadening' model. The dash–dot–dot line stands for the excess yield defined by the total yield (for the 'collisional broadening' scenario) after subtraction of the HSD 'cocktail'. As seen from Fig. 4, in addition to the ρ meson contribution the HSD excess yield shows an enhancement at low invariant mass which is related to other dilepton sources not included in the 'cocktail', in particular to a sizeable contribution from the Δ Dalitz decay. The HSD excess yields show a reasonable agreement with the CERES data in the 'collisional broadening' scenario and in the 'dropping mass + collisional broadening' model except of the first data point, which we relate more to uncertainties in the definition of the 'hadronic cocktail' than to new effects. More precise experimental data at very low mass as well as improvements of the 'cocktail' will shed more light on this issue.

We step on to RHIC energies and first compare the HSD results for the dilepton invariant mass spectrum from *pp* collisions at $\sqrt{s} = 200$ GeV with the data from PHENIX [40] in Fig. 5. The electron–positron pairs simulated in each *pp* event have been passed through the PHENIX acceptance and mass resolution routines [40]. We note that HSD for (inelastic) *pp* reactions for $\sqrt{s} > 2.6$ GeV is identical to FRITIOF (including PYTHIA v5.5 with JETSET v7.3 for the production and fragmentation of jets), i.e. for general hadron production. Explicit comparisons with data for *pp* reactions are presented in Refs. [41] as well as in Ref. [42] (Fig. 1). Since
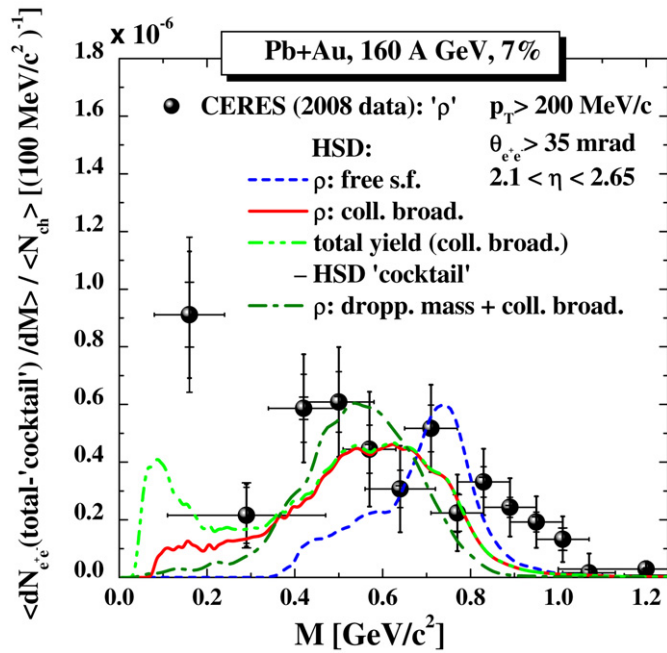
Fig. 4. The comparison of the CERES data for the dilepton yield after subtraction of the hadronic cocktail (without the ρ) [22] with the HSD calculations: the dashed line shows the result for the vacuum ρ spectral function whereas the solid line corresponds to the 'collisional broadening' scenario; the dash–dot–dot line stands for the excess yield defined as total yield after HSD 'cocktail' subtraction. The dash-dotted line represents the HSD calculations for the 'dropping mass + collisional broadening' model.
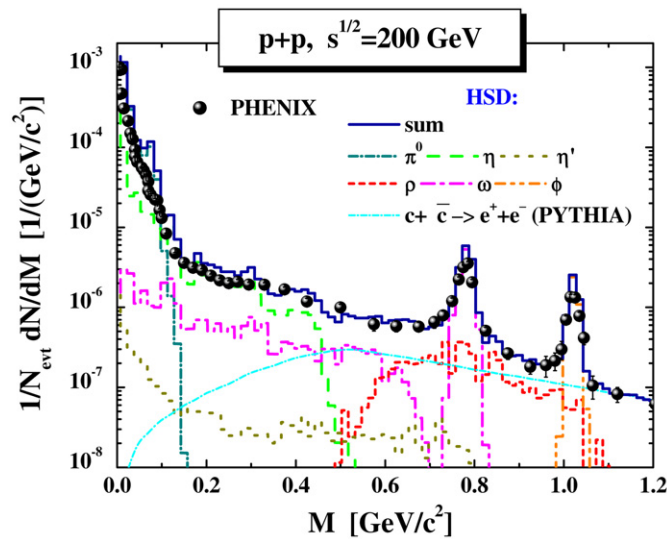

Fig. 5. The HSD results for the mass differential dilepton spectra in case of pp collisions at $\sqrt{s} = 200$ GeV in comparison to the data from PHENIX [40]. The actual PHENIX acceptance and mass resolution have been incorporated (see legend for the different color coding of the individual channels).

FRITIOF is modeled (fixed) to describe accurately elementary channels such as pp or $\pi + p$ reactions also HSD performs in a similar way.

As seen from Fig. 5 the HSD calculations well reproduce the PHENIX experimental spectrum which can entirely be described by meson Dalitz and direct decays as well as some contribution from open charm decays (light blue thin solid line as calculated by PYTHIA). This comparison demonstrates that the hadron production channels in HSD for elementary pp collisions are well under control also at the top RHIC energy.
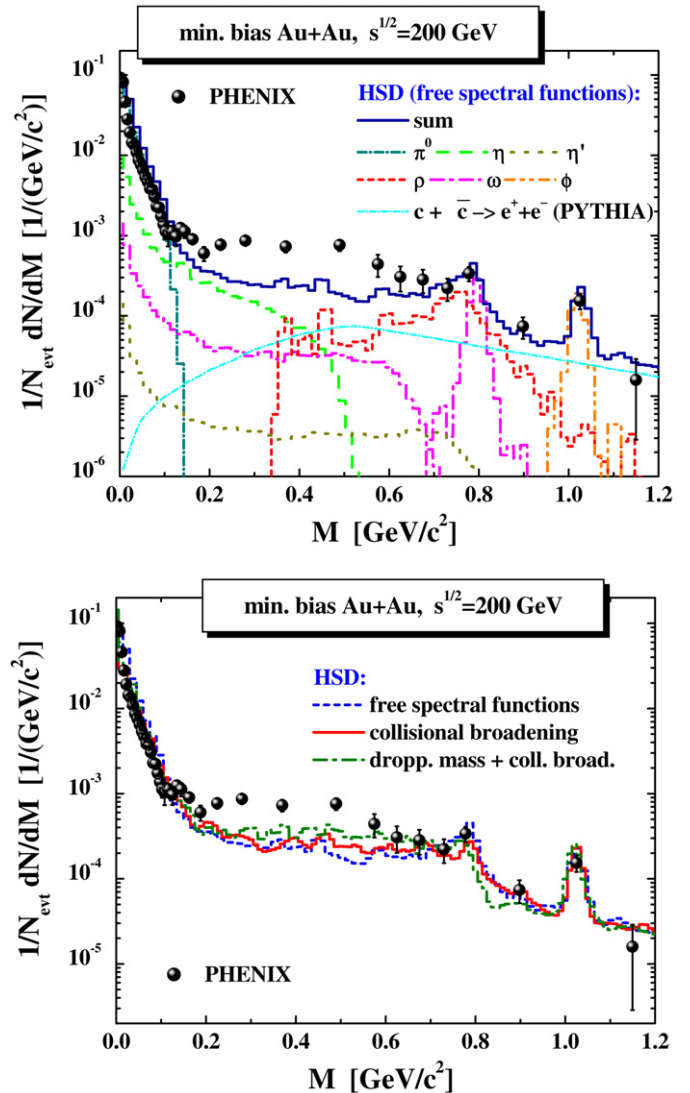

Fig. 6. The HSD results for the mass differential dilepton spectra in case of inclusive $Au + Au$ collisions at $\sqrt{s} = 200$ GeV in comparison to the data from PHENIX [23]. The actual PHENIX acceptance filter and mass resolution have been incorporated [43]. In the upper part the results are shown for vacuum spectral functions (for ρ, ω, ϕ) including the channel decompositions (see legend for the different color coding of the individual channels). The lower part shows a comparison for the total e^+e^- mass spectrum in case of the 'free' scenario (dashed line), the 'collisional broadening' picture (solid line) as well as the 'dropping mass + collisional broadening' model (dash-dotted line).

We recall that HSD also provides a reasonable description of hadron production in $Au + Au$ collisions at $\sqrt{s} = 200$ GeV [41] such that we can directly continue with the results for e^+e^- pairs which are shown in Fig. 6 in case of inclusive $Au + Au$ collisions in comparison to the data from PHENIX [23]. Again the actual PHENIX acceptance filter and mass resolution have been incorporated [43]. In the upper part of Fig. 6 the results are shown for vacuum spectral functions (for ρ, ω, ϕ) including the channel decompositions (see legend for the different color coding of the individual channels). Whereas the total yield (upper solid line) is quite well described in the region of the pion Dalitz decay as well as the ω and ϕ mass regime we clearly underestimate the measured spectra in the regime from 0.2 to 0.6 GeV by an average factor of 3.

When including the 'collisional broadening' scenario for the vector mesons we achieve the sum spectrum shown by the solid line in the lower part of Fig. 6 which is only slightly enhanced compared to the 'free' scenario (dashed line). Thus the question

emerges if the PHENIX data might signal dropping vector meson masses? To answer this question we have performed also calculations in the 'dropping mass + collisional broadening' model where the ρ and ω masses have been dropped with baryon density in accordance with Eq. (10) in Ref. [28]. The respective HSD results are displayed in the lower part of Fig. 6 by the dash-dotted line and indeed show a further enhancement of the dilepton yield which, however, is only small in the mass range 0.2 GeV $< M <$ 0.4 GeV such that also this possibility has to be excluded in comparison to the PHENIX data.

In summary we have used the off-shell version of the relativistic HSD transport model for the calculation of dilepton spectra from elementary as well as nucleus–nucleus collisions. Whereas the presently available dilepton data at SIS energies of 1 to 2 A GeV (from the HADES Collaboration [44]) are well described in the 'collisional broadening' scenario [28] this also holds for low mass dimuon data from In + In collisions at 158 A GeV (from the NA60 Collaboration) as well as the low mass dilepton spectra for Pb + Au collisions at 40 and 158 A GeV (from the CERES Collaboration). The 'dropping mass + collisional broadening' model for vector mesons seems compatible with the CERES data at SPS energies but does not perform well for the NA60 data. However, the low mass dilepton spectra from Au + Au collisions at RHIC (from the PHENIX Collaboration) are clearly underestimated in the invariant mass range from 0.2 to 0.6 GeV in the 'collisional broadening' scenario as well as in the 'dropping mass + collisional broadening' model, i.e. when assuming a shift of the vector meson mass poles with the baryon density. We mention that our results for the low mass dileptons are very close to the calculated spectra from van Hees and Rapp as well as Dusling and Zahed [45] (cf. the comparison in Ref. [46]). Consequently we attribute this additional low mass enhancement seen by PHENIX to non-hadronic sources, possibly to virtual gluon-Compton scattering [47].

Acknowledgement

References

[1] G.E. Brown, M. Rho, Phys. Rev. Lett. 66 (1991) 2720;
    G.E. Brown, M. Rho, Phys. Rep. 363 (2002) 85.
[2] T. Hatsuda, S. Lee, Phys. Rev. C 46 (1992) R34.
[3] M. Asakawa, C.M. Ko, Phys. Rev. C 48 (1993) R526.
[4] C.M. Shakin, W.-D. Sun, Phys. Rev. C 49 (1994) 1185.
[5] F. Klingl, W. Weise, Nucl. Phys. A 606 (1996) 329;
    F. Klingl, N. Kaiser, W. Weise, Nucl. Phys. A 624 (1997) 527.
[6] S. Leupold, W. Peters, U. Mosel, Nucl. Phys. A 628 (1998) 311.
[7] R. Rapp, G. Chanfray, J. Wambach, Phys. Rev. Lett. 76 (1996) 368.
[8] B. Friman, H.J. Pirner, Nucl. Phys. A 617 (1997) 496.
[9] R. Rapp, G. Chanfray, J. Wambach, Nucl. Phys. A 617 (1997) 472.
[10] W. Peters, M. Post, H. Lenske, S. Leupold, U. Mosel, Nucl. Phys. A 632 (1998) 109;
    M. Post, S. Leupold, U. Mosel, Nucl. Phys. A 689 (2001) 753.
[11] W. Cassing, E.L. Bratkovskaya, Phys. Rep. 308 (1999) 65.
[12] R. Rapp, J. Wambach, Adv. Nucl. Phys. 25 (2000) 1.
[13] G. Agakichiev, et al., CERES Collaboration, Phys. Rev. Lett. 75 (1995) 1272;
    Th. Ullrich, et al., Nucl. Phys. A 610 (1996) 317c;
    A. Drees, Nucl. Phys. A 610 (1996) 536c.
[14] M.A. Mazzoni, HELIOS Collaboration, Nucl. Phys. A 566 (1994) 95c;
    M. Masera, Nucl. Phys. A 590 (1995) 93c;
    T. Åkesson, et al., Z. Phys. C 68 (1995) 47.
[15] G.Q. Li, C.M. Ko, G.E. Brown, Phys. Rev. Lett. 75 (1995) 4007.
[16] C.M. Ko, G.Q. Li, G.E. Brown, H. Sorge, Nucl. Phys. A 610 (1996) 342c.
[17] W. Cassing, W. Ehehalt, C.M. Ko, Phys. Lett. B 363 (1995) 35.
[18] E.L. Bratkovskaya, W. Cassing, Nucl. Phys. A 619 (1997) 413.
[19] C. Ernst, et al., Phys. Rev. C 58 (1998) 447.
[20] W. Cassing, E.L. Bratkovskaya, R. Rapp, J. Wambach, Phys. Rev. C 57 (1998) 916.
[21] R. Arnaldi, et al., NA60 Collaboration, Phys. Rev. Lett. 96 (2006) 162302;
    J. Seixas, et al., J. Phys. G 34 (2007) S1023;
    S. Damjanovic, et al., Nucl. Phys. A 783 (2007) 327c.
[22] D. Adamova, et al., CERES Collaboration, Nucl. Phys. A 715 (2003) 262;
    D. Adamova, et al., CERES Collaboration, Phys. Rev. Lett. 91 (2003) 042301;
    G. Agakichiev, et al., Eur. Phys. J. C 41 (2005) 475;
    D. Adamova, et al., nucl-ex/0611022;
    A. Marin, et al., PoS CPOD07 (2007) 034, arXiv: 0802.2679 [nucl-ex].
[23] A. Toia, et al., PHENIX Collaboration, Nucl. Phys. A 774 (2006) 743;
    A. Toia, et al., PHENIX Collaboration, Eur. Phys. J. 49 (2007) 243;
    S. Afanasiev, et al., arXiv: 0706.3034 [nucl-ex].
[24] W. Ehehalt, W. Cassing, Nucl. Phys. A 602 (1996) 449.
[25] B. Anderson, G. Gustafson, H. Pi, Z. Phys. C 57 (1993) 485.
[26] T. Falter, et al., Phys. Lett. B 594 (2004) 61;
    T. Falter, et al., Phys. Rev. C 70 (2004) 054609.
[27] W. Cassing, S. Juchem, Nucl. Phys. A 665 (2000) 377;
    W. Cassing, S. Juchem, Nucl. Phys. A 672 (2000) 417.
[28] E.L. Bratkovskaya, W. Cassing, Nucl. Phys. A 807 (2008) 214.
[29] K. Haglin, Nucl. Phys. A 584 (1995) 719.
[30] M. Floris, et al., NA60 Collaboration, J. Phys., Conf. Series 5 (2005) 55.
[31] S. Damjanovic, private communication.
[32] H. van Hees, R. Rapp, Phys. Rev. Lett. 97 (2006) 102301.
[33] H. van Hees, R. Rapp, Nucl. Phys. A 806 (2008) 339.
[34] W. Cassing, Talk presented at the CERN TH Workshop on Electromagnetic Radiation in Nuclear Collisions, http://ph-dep-th.web.cern.ch/ph-dep-th/?site=content2/workshops/HIworkshopElmag/HIworkshopElmag.html.
[35] R. Rapp, J. Phys. G 34 (2007) S405;
    R. Rapp, Nucl. Phys. A 782 (2007) 275.
[36] J. Ruppert, C. Gale, T. Renk, P. Lichard, J.I. Kapusta, Phys. Rev. Lett. 100 (2008) 162301.
[37] C. Gale, S. Turbide, Nucl. Phys. A 783 (2007) 351.
[38] J. Ruppert, T. Renk, Phys. Rev. C 71 (2005) 064903;
    J. Ruppert, T. Renk, Phys. Rev. C 75 (2007) 059901, Erratum;
    T. Renk, J. Ruppert, hep-ph/0605130.
[39] K. Dusling, D. Teaney, I. Zahed, Phys. Rev. C 75 (2007) 024908.
[40] A. Adare, et al., PHENIX Collaboration, arXiv: 0802.0050 [nucl-ex].
[41] E.L. Bratkovskaya, W. Cassing, H. Stöcker, Phys. Rev. C 67 (2003) 054905;
    E.L. Bratkovskaya, et al., Phys. Rev. C 69 (2004) 054907.
[42] W. Cassing, et al., Nucl. Phys. A 735 (2004) 277.
[43] A. Toia, private communication.
[44] J. Pietraszko, et al., HADES Collaboration, Int. J. Mod. Phys. A 22 (2007) 388;
    G. Agakichiev, et al., Phys. Rev. Lett. 98 (2007) 052302;
    T. Eberl, et al., HADES Collaboration, Eur. Phys. J. C 49 (2007) 261;
    G. Agakishiev, et al., Phys. Lett. B 663 (2008) 43;
    Y.C. Pachmayer, et al., arXiv: 0804.3993 [nucl-ex].
[45] K. Dusling, I. Zahed, arXiv: 0712.1982 [nucl-th].
[46] A. Toia, arXiv: 0805.0153 [nucl-ex].
[47] O. Linnyk, E.L. Bratkovskaya, W. Cassing, in preparation.